Theoretical study of near edge electron energy loss spectroscopy of metal nanoclusters

2006 J. Phys.: Condens. Matter 18 1211

(http://iopscience.iop.org/0953-8984/18/4/009)

INSTITUTE OF PHYSICS PUBLISHING JOURNAL OF PHYSICS: CONDENSED MATTER

J. Phys.: Condens. Matter **18** (2006) 1211–1226 doi:10.1088/0953-8984/18/4/009

Theoretical study of near edge electron energy loss spectroscopy of metal nanoclusters

Michele Gusso

ENEA - Ente per le Nuove Tecnologie l' Energia e l' Ambiente, Unitá Materiali e Nuove Tecnologie, CR Brindisi, SS 7 Appia km 714, I-72100 Brindisi, Italy

E-mail: michele.gusso@brindisi.enea.it

Received 1 September 2005, in final form 13 November 2005
Published 11 January 2006
Online at stacks.iop.org/JPhysCM/18/1211

Abstract

The near edge structure of the electron energy loss spectra (ELNES) of copper and gold clusters containing up to 923 atoms are theoretically studied with the multiple scattering approach in the framework of density functional theory. Calculations are performed both in the atomic sphere approximation (ASA) and in the full potential (FP) framework and their results compared. The effects of structure relaxation of the clusters on the ELNES are assessed. Finally an example of the ELNES of a Cu–Ag core shell nanocrystal is given.

1. Introduction

Nanoclusters have received much attention due to their unique physical and chemical properties. Among the techniques used for their characterization, transmission electron microscopy (TEM) plays a major role with its unique capability of giving analytical and structural information with atomic spatial resolution. Structural information is mainly obtained with high-resolution transmission electron microscopy images (HRTEM) [1], diffraction patterns and Z-contrast scanning transmission electron microscopy (STEM) images [2], while electron energy loss spectroscopy (EELS) can be used in order to obtain elemental information at an atomic scale. In particular, the near edge structure (ELNES) of a core level excitation of an atomic element is sensitive to the structural and chemical environment of that element. The advent of modern transmission electron microscopes equipped with high-brilliance sources, such as field emission guns, allows the recording of ELNES from single nanoclusters or even from different regions of the same nanocluster if a STEM or a TEM equipped with an imaging energy filter is used. These characteristics make ELNES an appealing tool for determining the physical and chemical properties of nanoclusters and in particular their surface characteristics, which are difficult to obtain with other techniques.

Despite its great potential for giving structural and chemical information on the nature of nanoclusters, ELNES does not appear very often in the literature of these materials and in any case the large amount of information contained in these spectra is rarely exploited. The main

reason for this lies in the difficulty of interpreting an ELNES spectrum which, most of the time, can only be achieved by a comparison with simulated spectra. Since an ELNES spectrum is the result of an excitation process, a rigorous simulation would require the use of theoretical tools such as two-particle Green's function theory (solution of the Bethe–Salpeter equation) or time-dependent density functional theory (TDDFT) [3]. Although TDDFT has undergone important advances in recent years, its applicability to complex systems (i.e. systems with many inequivalent atoms in the unit cell) still requires a considerable and often insurmountable computational effort. The use of these techniques is necessary in order to simulate the many-body effects that are present during excitation processes. On the other hand, when a core electron is excited the most important of such effects is the so-called core hole effect that can sometimes be mimicked by the use of simple approximations such as the $Z + 1$ approximation. In this way good simulations can be obtained by simply using standard density functional theory (DFT) [4].

In this work we treat the excitation of a core electron by a fast incident electron within DFT. We fix our attention on the theoretical simulation of ELNES of Cu and Au nanocrystals containing up to 923 atoms with cuboctahedral symmetry. It has been shown [5] that, from a computational point of view, the study of nanoclusters is easier if a real space approach is used; in this paper we calculate the ELNES within the multiple scattering (MS) formalism (precisely, we use a real space formulation of the screened Korringa–Kohn–Rostoker (KKR) method [14]). In section 2 general expressions to calculate ELNES in the MS formalism are reported. In section 3 we discuss some technical aspects of the computation, and in particular we show how the rotational symmetry of the clusters considered is exploited in order to speed up the calculation and decrease the amount of memory required for the computation. Section 4 reports the results. First we show the effects of nanocluster size on the ELNES features. Then we assess the validity of some approximations. We show the difference between a self-consistent field (SCF) calculation performed with full potentials (FP) instead of adopting the atomic sphere approximation (ASA) [6]. Then the effects on the ELNES spectra of the structure relaxation of nanoclusters is considered. Finally we report an example of a cluster composed of a Cu core surrounded by a shell of Ag atoms. Section 5 contains the conclusions.

2. Theory

Treating the fast incident electron as a plane wave and using the first Born approximation, the EELS signal is given by the double differential scattering cross section [7, 8]:

$$\frac{\partial^2\sigma}{\partial\Delta E\partial\Omega} = \frac{4\gamma^2}{q^4a_0^2}\frac{k}{k_0}S(\boldsymbol{q},\boldsymbol{q},\Delta E), \tag{1}$$

where $a_0 = 4\pi\varepsilon_0\hbar^2/me^2$ is the Bohr radius and $\gamma = (1-\beta^2)^{-1/2}$ is the relativistic factor. In this expression the diagonal part ($\boldsymbol{q} = \boldsymbol{q}'$) of the mixed dynamic form factor (MDFF) $S(\boldsymbol{q},\boldsymbol{q}',\Delta E)$ appears [9]. The wavevector $\boldsymbol{q}$ is such that $-\hbar\boldsymbol{q}$ is the momentum transferred to the scatterer in the inelastic interaction (i.e. $\boldsymbol{q} = \boldsymbol{k} - \boldsymbol{k_0}$, $\boldsymbol{k_0}$ and $\boldsymbol{k}$ being the wavevectors of the incident and scattered electrons, respectively). We now consider one-electron transitions and we write the mixed dynamic form factor $S(\boldsymbol{q},\boldsymbol{q}',\Delta E)$ as the Fourier transform of the real space MDFF (rMDFF) [8]

$$S(\boldsymbol{r},\boldsymbol{r}',\Delta E) = \int_{\varepsilon_F-\Delta E}^{\varepsilon_F}\rho_i(\boldsymbol{r},\boldsymbol{r}',\varepsilon)\rho_f(\boldsymbol{r}',\boldsymbol{r},\varepsilon+\Delta E)\,\mathrm{d}\varepsilon, \tag{2}$$

where $\rho_i(\boldsymbol{r},\boldsymbol{r}',\varepsilon)$ and $\rho_f(\boldsymbol{r},\boldsymbol{r}',\varepsilon)$ are the energy-dependent density matrices of the target initial state and final state, respectively, and ε_F is the Fermi energy. Thus, the rMDFF is

the energy correlation function between the density matrices of occupied (initial) states and unoccupied (final) states, with energy difference ΔE between these states. ΔE equals the energy loss of the probe electron.

The density matrix is related to the one-electron Green's function by the relation:

$$\rho(\boldsymbol{r}, \boldsymbol{r}', E) = -\frac{2}{\pi} \operatorname{Im} G(\boldsymbol{r}, \boldsymbol{r}', E). \tag{3}$$

Therefore, if the Green's function of a material system is known, its EELS spectrum can be computed. In the following we will restrict our calculation to the muffin tin (MT) approximation for the derivation of the expression of the ELNES intensity. The results for a general FP treatment are quoted in the appendix. The following results are also valid for complex energies.

In multiple scattering theory the Green's function G is calculated by solving the Lippmann–Schwinger equation for G (see for example [10, 11]) in an effective potential which is the one that appears in the Kohn–Sham equations [12]. The Green's function can be written in a mixed site-angular-momentum representation as

$$\begin{aligned} G(\boldsymbol{R_i} + \boldsymbol{r}, \boldsymbol{R_j} + \boldsymbol{r}', E) = {} & \sum_{LL'} R^i_L(r, E) Y_L(\hat{\boldsymbol{r}}) G^{ij}_{LL'}(E) R^j_L(r', E) Y_{L'}(\hat{\boldsymbol{r}}') \\ & + \delta_{ij} \sum_{L} R^i_L(r_<, E) Y_L(\hat{\boldsymbol{r}}) H^j_L(r_>, E) Y_L(\hat{\boldsymbol{r}}'), \end{aligned} \tag{4}$$

where $L \equiv (lm)$ are angular-momentum indices, $R^i_L(r, E)$ and $H^i_L(r_>, E)$ are properly normalized regular and irregular scattering solutions corresponding to the MT potential centred at position $\boldsymbol{R}_i$ [13], $r_>$ ($r_<$) denotes the greater (lesser) of r and r', $Y_L(\hat{\boldsymbol{r}})$ are real spherical harmonics and $G^{ij}_{LL'}$ are the elements of the structural Green's function matrix (for the calculation of these elements see equation (7) below). For spherically symmetric potentials, the normalization is chosen such that their asymptotic behaviour is

$$R^i_L(r, E) \sim j_l - \mathrm{i}\kappa t^i_l h_l, \tag{5}$$

$$H^i_L(r, E) \sim -\mathrm{i}\kappa h_l, \tag{6}$$

where $t^i_l = -1/\kappa \sin\delta^i_l \mathrm{e}^{\mathrm{i}\delta^i_l}$ is the atomic scattering matrix (δ^i_l are the scattering phase shifts of atom i, $\kappa = \sqrt{E}$ with E measured in rydberg), j_l are first kind spherical Bessel functions and h_l are spherical Hankel functions. For the calculation of the structural Green's function matrix $\mathbf{G}(E) = \{G^{ij}_{LL'}(E)\}$ it is useful to introduce a reference system r made of new scattering centres with potentials V^r located in the same positions as the real scattering centres [14]. Denoting by $\mathbf{t^r}(E)$ and $\mathbf{G^r}(E)$ the atomic scattering matrices and the structural Green's function matrices of this reference system r, we have the following relation which relates the structural Green's function of the two systems:

$$\mathbf{G}(E) = \mathbf{G^r}(E)(\mathbf{I} - \boldsymbol{\Delta}\mathbf{t}(E)\mathbf{G^r}(E))^{-1}, \tag{7}$$

where $\mathbf{I}$ is the identity matrix and we have introduced

$$\boldsymbol{\Delta}\mathbf{t}(E) = \mathbf{t}(E) - \mathbf{t^r}(E). \tag{8}$$

If the potentials V^r are zero everywhere we have the vacuum as reference system. A good choice [14] is to take constant repulsive muffin tin potentials arranged on the sites of the real system (for example potential wells with $V^r = 4$ or 8 Ryd). In this way it can be shown that the structural Green's function $\mathbf{G^r}(E)$ is short ranged (i.e. it decays exponentially with the distance $|\boldsymbol{R}_i - \boldsymbol{R}_j|$ between two sites). Consequently the structural Green's function matrix of the real

system $\mathbf{G}(E)$ is obtained from equation (7) by inversion of a sparse matrix. The matrix $\mathbf{G^r}(E)$ is obtained by an equation analogous to (7):

$$\mathbf{G^r}(E) = \mathbf{G^0}(E)(\mathbf{I} - \mathbf{t^r}(E)\mathbf{G^0}(E))^{-1}, \tag{9}$$

where $\mathbf{G^0}(E)$ is the structural Green's function matrix of free space. It can be shown [14] that accurate results for the elements $G^{r,ij}_{LL'}(E)$ of the matrix $\mathbf{G^r}(E)$ are obtained even if we take a small cluster of muffin tin potentials around each atom (for example, a cluster of 19 muffin tin potentials around each atom is sufficient to get accurate results for copper). Therefore the calculation of the structural Green's function of the reference system requires little effort and is particularly convenient when a material with a lot of atoms in the unit cell is being studied.

We now consider the case of an excitation of a core electron whose wavefunction is assumed to be well described by an atomic wavefunction completely sharp in energy. We also assume that all other core levels are sufficiently separated in energy from the one we are considering, so that their contribution to ELNES (i.e. integral in energy in (2)) can be neglected. The density matrix of the core electrons with angular momentum l is given by

$$\rho(\boldsymbol{r}, \boldsymbol{r}', E^i_c) = 2\sum_m R^{ic}_l(r, E^i_c)Y_L(\hat{\boldsymbol{r}})R^{ic}_l(r', E^i_c)Y_L(\hat{\boldsymbol{r}}'), \tag{10}$$

where R^{ic}_l are real core electron functions of the atom i corresponding to the energy level E^i_c and the factor 2 comes from the sum over spins.

Inserting equations (3), (4) and (10) in (2) we have:

$$\begin{aligned} S(\boldsymbol{q}, \boldsymbol{q}, E) = -\frac{2}{\pi}\sum_i \int \mathrm{d}^3 r \int \mathrm{d}^3 r' \sum_L R^{ic}_l(r, E^i_c)Y_L(\hat{\boldsymbol{r}})R^{ic}_l(r', E^i_c)Y_L(\hat{\boldsymbol{r}}') \\ \times \mathrm{Im}\Bigg[\sum_{LL'} R^i_l(r, E)Y_L(\hat{\boldsymbol{r}})G^{ii}_{LL'}(E)R^i_l(r', E)Y_{L'}(\hat{\boldsymbol{r}}') \\ + \sum_L R^i_l(r_<, E)Y_L(\hat{\boldsymbol{r}})H^i_l(r_>, E)Y_L(\hat{\boldsymbol{r}}')\Bigg]\mathrm{e}^{-\mathrm{i}\boldsymbol{q}\boldsymbol{r}}\mathrm{e}^{\mathrm{i}\boldsymbol{q}\boldsymbol{r}'}. \end{aligned} \tag{11}$$

Since the core electron functions of an atom are localized near the atom itself we only need to consider the site diagonal elements of G^{ij}. In the electric dipole approximation we expand the terms $\mathrm{e}^{-\mathrm{i}\boldsymbol{q}\boldsymbol{r}}$ to first order in $\boldsymbol{q}\boldsymbol{r}$. By rearranging the integrals we have:

$$S(\boldsymbol{q}, \boldsymbol{q}, \Delta E) = \frac{-4}{\pi}\,\mathrm{Im}\sum_i \left[\sum_{mL'} M^{iB}_{LL'}(\boldsymbol{q}) + \sum_{mL'L''} M^{iA}_{LL''}(\boldsymbol{q})G^{ii}_{L'L''}M^{iA}_{LL'}(\boldsymbol{q})\right], \tag{12}$$

where

$$\begin{aligned} M^{iA}_{LL'}(\boldsymbol{q}) &= \int \mathrm{d}\boldsymbol{r}\, R^{ic}_l(r, E^i_c)Y_L(\hat{\boldsymbol{r}})(\boldsymbol{q}\boldsymbol{r})R^i_{l'}(r, E)Y_{L'}(\hat{\boldsymbol{r}}) \\ M^{iB}_{LL'}(\boldsymbol{q}) &= 2\int\int R^{ic}_l(r, E^i_c)Y_L(\hat{\boldsymbol{r}})(\boldsymbol{q}\boldsymbol{r})R^i_{l'}(r, E)Y_{L'}(\hat{\boldsymbol{r}}) \\ &\quad \times R^{ic}_l(r', E^i_c)Y_L(\hat{\boldsymbol{r}}')(\boldsymbol{q}\boldsymbol{r}')H^i_{l'}(r', E)Y_{L'}(\hat{\boldsymbol{r}}') \\ &\quad \times \theta(r - r')\,\mathrm{d}\boldsymbol{r}\,\mathrm{d}\boldsymbol{r}'. \end{aligned} \tag{13}$$

Here $\theta(r)$ is the step function. In the appendix we report the expressions for the double differential scattering cross section in the case where a full potential treatment is used instead of the muffin tin approximation. Expressions (12) and (14) are the MS results that corresponds to the relations reported in [15] obtained in the augmented plane wave approach. Similar expressions for x-ray absorption spectra were obtained within the MS theory but with

various approximations: for real energies and with the muffin tin approximation [16], for real energies and with the full potential treatment [17] and for complex energies and the muffin tin approximation [18, 19].

The spectrum acquired in a TEM is obtained by recording the electrons scattered by the specimen that pass through a spherical aperture. Therefore we have to integrate the expressions (13) over the scattering wavevector $\boldsymbol{q}$ from a $q_{\min} = k_i\theta_E$ to a $q_{\max} = k_i(\theta_{\max}^2 + \theta_E^2)^{1/2}$, where $\theta_E = \Delta E(E + E_M)/E(E + 2E_M)$ with E_M the electron rest energy and $\theta_{\max}$ the maximum angle that the scattered electrons entering the aperture form with the incident electrons. Using the results of [20] for the integration over $\boldsymbol{q}$ we have (supposing the aperture to be in the xy plane with the z-axis parallel to the incident beam)

$$\begin{aligned}\frac{\partial\sigma(\Delta E, q_{\min}, q_{\max})}{\partial\Delta E} = \frac{-16\gamma^2}{a_0^2}\frac{1}{k_0^2}\mathrm{Im}\Bigg[\sum_i\sum_{mL'}\Bigg(&\ln\frac{q_{\max}}{q_{\min}}(M^{iBxx}_{LL'} + M^{iByy}_{LL'}) \\ &+ A(2M^{iBzz}_{LL'} - M^{iBxx}_{LL'} - M^{iByy}_{LL'})\Bigg) \\ &+ \sum_{mL'L''}\Bigg(\ln\frac{q_{\max}}{q_{\min}}(M^{iAx}_{LL'}G^{ii}_{L'L''}M^{iAx}_{LL''} + M^{iAy}_{LL'}G^{ii}_{L'L''}M^{iAy}_{LL''}) \\ &+ A(2M^{iAz}_{LL'}G^{ii}_{L'L''}M^{iAz}_{LL''} - M^{iAx}_{LL'}G^{ii}_{L'L''}M^{iAx}_{LL''} \\ &- M^{iAy}_{LL'}G^{ii}_{L'L''}M^{iAy}_{LL''})\Bigg)\Bigg],\end{aligned} \tag{14}$$

where

$$A = \frac{2m}{8\hbar^2}\frac{\Delta E^2}{E_0}\left(\frac{1}{q_{\min}^2} - \frac{1}{q_{\max}^2}\right) + \frac{\Delta E}{2E_0}\ln\frac{q_{\max}}{q_{\min}} + \frac{1}{8}\frac{\hbar^2}{2mE_0}(q_{\max}^2 - q_{\min}^2) \tag{15}$$

with $E_0 = \hbar^2k_0^2/2m$ and $\Delta E = \hbar^2(k_0^2 - k^2)/2m$ the energy lost by the incident electron and

$$\begin{aligned}M^{iAx}_{LL'} &= \int \mathrm{d}\boldsymbol{r}\, R^{ic}_l(r, E^i_c)Y_L(\hat{\boldsymbol{r}})x\,R^i_{l'}(r, E)Y_{L'}(\hat{\boldsymbol{r}}) \\ M^{iBxx}_{LL'} &= 2\int\int R^{ic}_l(r, E^i_c)Y_L(\hat{\boldsymbol{r}})x\,R^i_{l'}(r, E)Y_{L'}(\hat{\boldsymbol{r}}) \\ &\quad\times R^{ic}_l(r', E^i_c)Y_L(\hat{\boldsymbol{r}}')x'H^i_{l'}(r', E)Y_{L'}(\hat{\boldsymbol{r}}')\theta(r - r')\,\mathrm{d}\boldsymbol{r}\,\mathrm{d}\boldsymbol{r}',\end{aligned} \tag{16}$$

with analogous obvious definitions for the other matrix elements M. Writing the Cartesian coordinates x, y and z in a polar reference system, the integrals (16) can be easily factorized into a radially dependent and an angular-dependent part. The last one determines the dipole selection rule and can be expressed in terms of Wigner symbols. Equation (14) is the ELNES expression that will be used in all the examples reported in section 4 when the ASA approximation is used, while for a FP treatment the relations reported in the appendix are considered. Note that the total ELNES signal of a cluster of atoms can be decomposed into separate contributions from the single atoms forming the cluster. Note also that since in equation (14) we have integrated over a spherical aperture positioned in the xy plane, any possible anisotropy of the scattering cross section with respect to $\boldsymbol{q}$ in this plane is lost. Instead a possible anisotropy in the q_z with respect to the q_{xy} direction is still present due to the different weights in equation (14) of the M^{iAz} and M^{iBz} matrix elements with respect to the xy ones.

3. Computational aspects

In order to study the dependence of the ELNES on the cluster dimension we have focused our attention on nanocrystals with cuboctahedral symmetry made of copper or gold with an increasing number of atoms. For each cluster, we have first calculated the ground state charge density and the Kohn–Sham effective potential in a SCF way using the MS approach and then the ELNES spectrum using the expressions described in the previous section. We have considered the following sequence of magic numbers: 13, 55, 147, 309, 561, 923. To account for the spilling of the electron charge into the vacuum region in the SCF cycles, each cluster was surrounded by empty spheres located in the atomic positions of the cluster two positions next in the sequence. So, for example, a cluster of 55 Cu atoms was surrounded by empty spheres so as to have a cuboctahedral cluster with a total of 309 atoms (55 Cu atoms +254 empty spheres). In the following the notation Cu55 will be used for the 55 Cu atom cluster, with obvious extension for all other kind of clusters. Exchange and correlation effects were treated in the local density approximation (LDA) with the Vosko, Wilk and Nusair parametrization of the exchange correlation potential [21]. The calculations were performed in the scalar relativistic approximation [22]. The core electrons were allowed to relax during the SCF cycles (i.e. no frozen core approximation was used). The maximum angular momentum used in the expansion of the Green's functions (equation (4)) was $l_{\max} = 3$ for Cu clusters and $l_{\max} = 4$ for Au clusters. The electron density in the SCF cycles was calculated from the Green's function by a contour integral in the complex energy plane. For the occupation function we used a Fermi–Dirac distribution with an electronic temperature of 400 K and the contour integral is evaluated with 21 complex energy points and three Matsubara poles [23]. For the calculation of the ELNES we considered a straight line parallel to the energy axis with a small imaginary part $\pi kT = 0.108$ eV which corresponds to $T = 400$ K, the temperature used in the self-consistent calculations. The calculation of the screened KKR parameters $\mathbf{G}^{\mathbf{r}ij}$ was obtained considering repulsive potentials of 8 Ryd height and with a coupling up to the second neighbour sites. An analysis of the convergence of the density of states with respect to the above-mentioned parameters ($l_{\max}$, number of complex energy points for the evaluation of the integral of the density of states, number of coupling atoms to calculate the screened structure constants $\mathbf{G}^{\mathbf{r}}$, height of the repulsive potentials), was performed on bulk copper and gold showing that the parameters used are good enough to obtain accurate results for both the ground state charge density and ELNES calculations, in view also of the fact that the ELNES intensity is then convoluted with a Lorentzian to account for the finite lifetime of the valence states and with a Gaussian in order to simulate the instrumental resolution. We also found that for the clusters considered the screening parameters used give accurate results in an energy range larger than for bulk calculations.

In order to study the dependence of the ELNES upon the relaxation of the clusters, we performed classical molecular dynamics simulations on two representative examples of the two series of clusters: Cu309 and Au309. We used a tight-binding second-moment approximation scheme [24]. In these cases the ASA radii used in the MS calculations were determined by calculating the local strain at each atomic site of the cluster (with respect to the unrelaxed case), and by changing the unrelaxed ASA radius by an amount proportional to the local strain.

The most difficult part of the computational procedure is the calculation of the matrix elements $G^{ii}_{LL'}(E)$ which are obtained by inverting the matrix given by equation (7). Different methods have been proposed to efficiently solve equation (7); among those deserving particular attention are Haydock's recursion method [25, 26], the local self-consistent multiple scattering method (LSMS) [27] and the locally self-consistent Green's function (LSGF) approach [28]. Since we have considered clusters with a well-defined point group symmetry (O_h), the

computational speed and the cluster size can be increased enormously if group representation theory is used [29, 30]. By using the projection operators of the point group O_h, basis states that transform according to one of its ten irreducible representations are formed. With respect to these basis states the matrix (7) becomes a block diagonal one. For example the matrix $14\,768 \times 14\,768$ of a cluster with 923 atoms and $l_{max} = 3$, is reduced to: four matrices with dimensions 363, 254, 296, 321 corresponding to the states A_{1g}, A_{1u}, A_{2g}, A_{2u} respectively; two identical 657-dimensional matrices for E_g states; two identical 572-dimensional matrices for E_u states; three identical 868-dimensional matrices for T_{1g} states; three identical 978-dimensional matrices for T_{1u} states; three identical 935-dimensional matrices for T_{2g} states; three identical 911-dimensional matrices for T_{2u} states. All calculations were done by modifying a screened KKR code originally written for computation of bulk and surface electronic properties [14].

To account for the finite lifetime of the valence states, the calculated ELNES spectra were convoluted with an energy-dependent Lorentzian with a broadening parameter $\Gamma = 0.1 \times \epsilon$, where ϵ is the energy of the excited electron calculated with respect to the Fermi level [31, 32]. In order to keep to a minimum the loss of information determined by the instrumental resolution and to allow a comparison with experiments performed with a modern field emission gun (FEG)-TEM equipped with a pre-specimen monochromator, we have further convoluted the data with a Gaussian having a full width at half maximum of only 0.2 eV.

It must be stressed that the effects of the core hole were never taken into account in the simulations presented in this work. We have avoided complicating the calculations for the following two reasons: for metals the effect of the core hole is less important than for semiconductors or insulators (although it is still present as has been reported in a study for copper [31] where, in particular, it is shown that it affects mainly the ELNES intensity in the first few electronvolts above the Fermi level); moreover we were mainly interested in showing the relative variation of the ELNES signal while changing some parameters (such as cluster size, cluster relaxation, ASA versus FP). Of course for a precise comparison with experimental data some modelling of the core hole (such as the $Z + 1$ approximation, Slater's transition state rule, etc) would be necessary. Finally it is to be noted that, because of the symmetry of the clusters considered in the present work, the value of the angle of the aperture used for recording the ELNES does not influence the shape of the spectrum and it simply determines a different overall scale factor (provided we consider collecting angles so that the dipole electric approximation is still valid).

4. Results and discussion

4.1. Dependence of ELNES on nanocluster size

Figure 1 shows the dependence of the Cu L_3 ELNES on the cluster size by considering six dimensions starting from Cu13 up to Cu923. In this and in all of the figures showing ELNES spectra, the zero of the energy is shifted so that it corresponds to the edge onset. In fact absolute edge onset values obtained with the use of LDA have errors of many electronvolts, so that they are not useful for comparison with experimental data. Some modelling of many body effects is necessary in order to obtain reliable values of edge onsets. Besides, to make comparison among ELNES spectra of clusters with different dimensions easier, in all the figures in this paper we always report the ELNES intensity normalized to the number of atoms of the cluster. It can be clearly seen that the cluster dimension strongly influences the shape of the spectrum: the number, height and position of the characteristic peaks of this edge. As the cluster size increases, the ELNES spectra become more and more similar.

In figure 1 we have also reported the ELNES of a cluster of 309 identical Cu atoms (labelled Cu309Bulk). For all atomic sites we have used the potential of a Cu atom in a fcc Cu

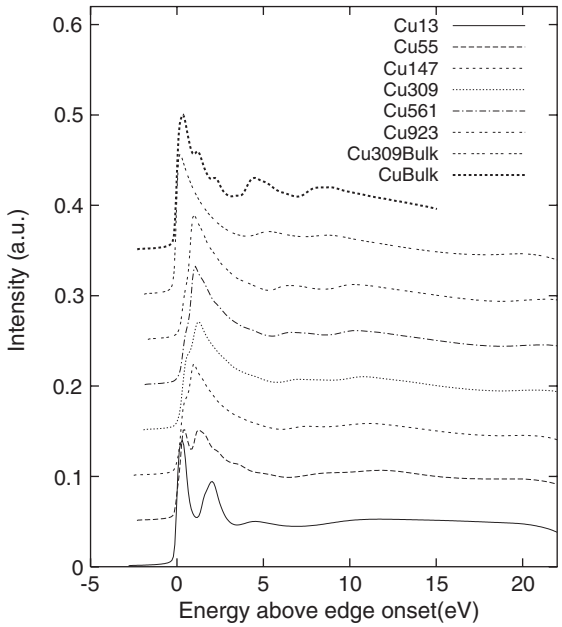

Figure 1. ELNES of the Cu L_3 edge for clusters Cu13, Cu55, Cu147, Cu309, Cu561, Cu923. The curve Cu309Bulk is the ELNES of a cluster of 309 identical Cu atoms with the potential of Cu bulk. The curve CuBulk is the ELNES of a Cu fcc crystal. To allow an easier comparison among the curves, each curve of the list (starting from Cu13) was shifted in the vertical direction by a constant value (=0.05) with respect to the previous one.

crystal. This spectrum is to be compared with that of Cu309 which has the same geometry. All the differences are due to a redistribution of the charge density inside the cluster and its spilling in the vacuum region. The differences between the two spectra are a clear indication of the importance of performing a SCF calculation.

As already said, the ELNES of a cluster is the sum of contributions from the single atoms forming the cluster. We have focused our attention on cluster Cu309 and we have reported in figure 2 the contributions to the ELNES from atoms in selected shells with increasing radii. Outer atoms present a smoother spectrum with respect to the inner ones, with a variation in position and height of the peaks. There is also an energy shift of the onset of the spectrum of each atom due to a variation of the energy level of the 2p core electrons (which are the electrons excited in this edge). In fact the binding energy of the core electrons decreases as we move towards atoms near the surface of the cluster. The variations of these energy levels range from 0 to 1.1 eV for ASA calculations of copper. For all these reasons the total spectrum of the cluster (which is reported in the bottom panel of figure 2), is generally less structured than that of the single atoms forming the cluster. For the same aforementioned reasons the ELNES tend to have generally fewer features while increasing the cluster size (since we have contributions from an increasing number of inequivalent atoms so that the sharp structures in the ELNES get smeared). Nevertheless, some peaks that could be almost absent in small nanoclusters can be found as the cluster size increases. This happens, for example, when these peaks are mainly caused by multiple scattering events of the excited electron with atoms far away from the excited one. Therefore they almost do not appear if the cluster is small. This seems to be the case of the peaks at 4 and 8 eV in the bulk spectrum which, although in a position shifted towards higher energies (with respect to the position in CuBulk), are better visible in the bigger

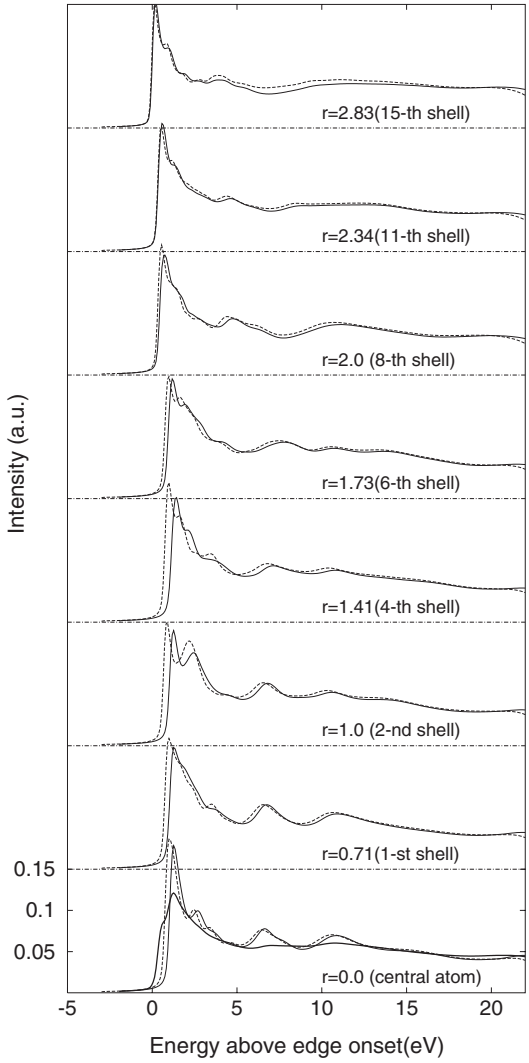

Figure 2. Contributions to the ELNES of the L_3 edge of cluster Cu309 from atoms with increasing distance from the centre. The radius r is given in units of the Cu bulk lattice parameter. The thin solid line refers to the ASA calculation while the dashed line refers to the FP result. For comparison, the total ELNES spectrum of the cluster obtained with the ASA approximation is reported in the bottom panel (thick solid line).

clusters than in the smaller ones. Hence, the combination of all these effects does not allow the prediction of a precise systematic trend.

A similar analysis has been performed for the O_3 edge of gold clusters. Figure 3 reports the ELNES for the clusters Au13 up to Au923, while figure 4 shows the contributions from selected atoms of cluster Au309. The same kind of considerations made for copper can be drawn also for Au clusters.

4.2. ASA versus FP calculations

It was shown [33] that the charge density obtained using the ASA approximation in a bulk material is very close to the density calculated with the FP method. But for atoms near the

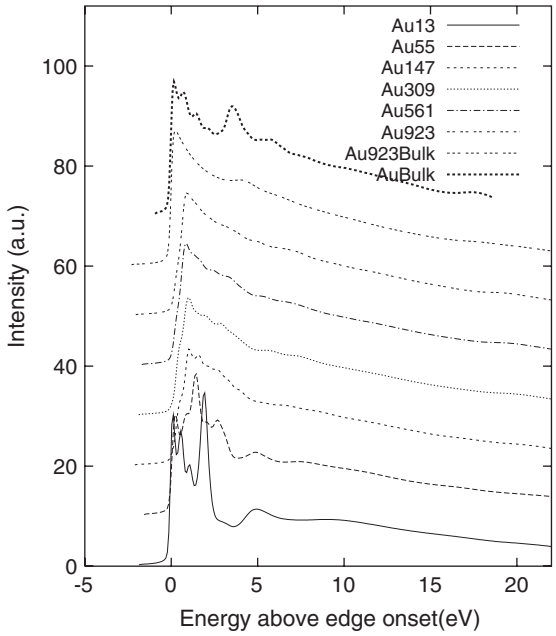

Figure 3. ELNES of the Au L_3 edge for clusters Au13, Au55, Au147, Au309, Au561, Au923. The curve Au309Bulk is the ELNES of a cluster of 309 identical Au atoms with the potential of Au bulk. The curve AuBulk is the ELNES of a Au fcc crystal. To allow for easier comparison among the curves, each curve of the list (starting from Au13) was shifted in the vertical direction by a constant value (=10) with respect to the previous one.

surface of the clusters there is a lowering of the local symmetry so that the charge density exhibits greater variation than in the bulk. In order to check the importance of going beyond a spherical approximation for the potential, we have performed SCF FP calculations on clusters with 55, 147 and 309 atoms and we have calculated the corresponding ELNES spectra using the expressions for the matrix elements reported in the appendix. Figures 2 and 4 show the ELNES contributions from selected atoms of clusters Cu309 and Au309, respectively, obtained using FP calculations and the ASA approximation. The spectra for atoms near the centre of the clusters are very similar (in particular for Cu309) apart from a different energy shift connected to a variation of the energy level of the core electron excited in this edge. For Cu309 the variation of the 2p core level energy for the atoms in the cluster is within 1.1 eV for ASA calculations and 0.8 eV for FP calculations. For Au309 the variation of the 5p core level energy is 0.8 eV in the ASA approximation and 0.9 eV for FP calculations. The resulting ELNES spectra for Cu and Au clusters are shown in figure 5. The comparison with the corresponding spectra obtained in the ASA approximation, also reported in the figures, shows that there are some slight variations which are more evident for Au clusters.

4.3. Effects of nanocluster relaxation on ELNES

Up to now we have considered cuboctahedral clusters obtained by cutting a portion of a perfect crystal. When left free to relax the atoms rearrange in order to minimize the free energy of the cluster. We have relaxed the structure of the clusters with molecular dynamics using tight-binding potentials in the second moment approximation [24] as described in section 3. Even if this in not an *ab initio* scheme, these potentials have been shown to give reliable results and

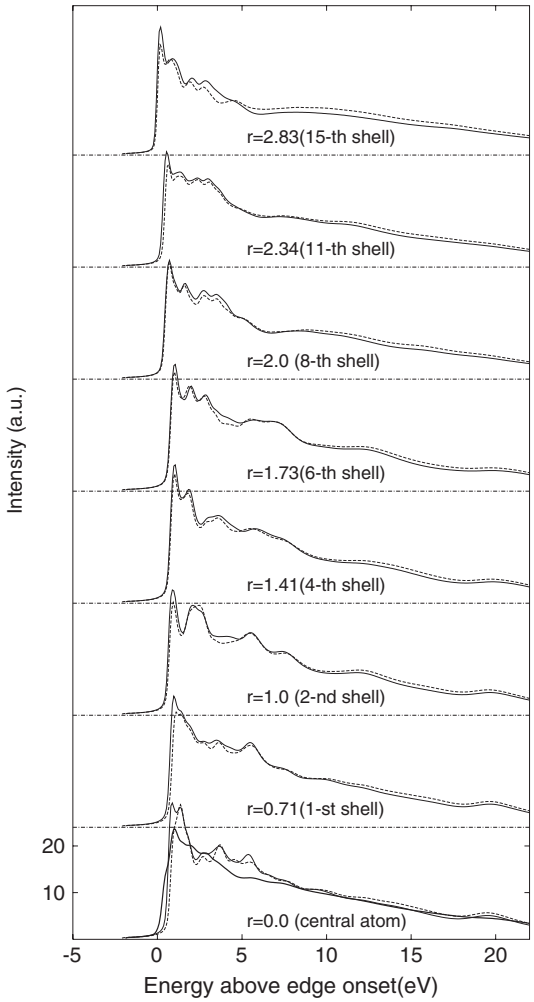

Figure 4. Contributions to the ELNES of the O_3 edge of cluster Au309 from atoms with increasing distance from the centre. The radius r is given in units of the Au bulk lattice parameter. The solid line refers to the ASA calculation while the dashed line refers to the FP result. For comparison, the total ELNES spectrum of the cluster obtained with the ASA approximation is reported in the bottom panel (thick solid line).

so can give us a good idea of the effects of relaxation on ELNES spectra. It is to be noted that after the relaxation, groups of rotationally equivalent atoms contract or expand by the same amount so that the relaxed cluster keeps the O_h point group symmetry. Figures 6 and 7 show a comparison of the ELNES for relaxed and unrelaxed Cu309 and Au309 clusters, respectively, in the ASA approximation. The relaxation yields some small changes in the spectrum of Cu309. In particular the shoulder at about 1 eV disappears after the relaxation. For Au309 the effects of relaxing the cluster are more important since they concern the shape of the whole spectrum.

4.4. Example of a CuAg core shell cluster

The clusters considered in the previous paragraphs were surrounded by a vacuum. We now consider an example of a Cu cluster surrounded by a layer of Ag atoms. We start with a core of Cu147 and suppose that we coherently grow on it a shell of 162 Ag atoms so as to have a

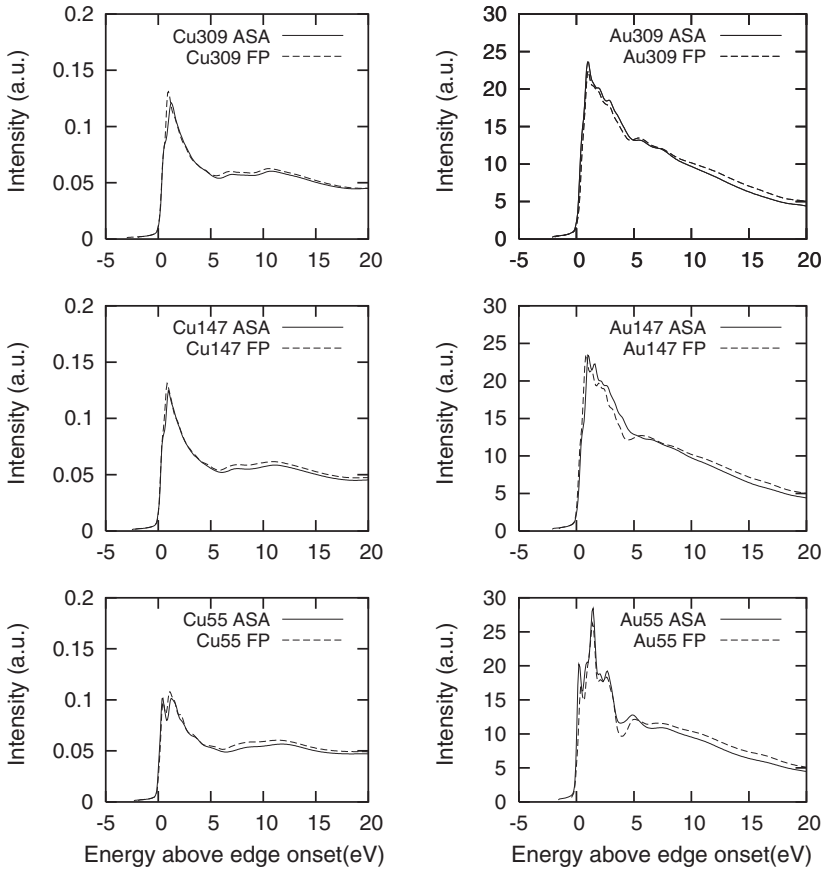

Figure 5. Comparison of the L_3 Cu edge and the O_3 Au edge simulated with a full potential (FP) calculation and using the atomic sphere approximations (ASA). On the left the spectra for clusters Cu55, Cu147 and Cu309 are reported, while on the right the spectra for clusters Au55, Au147 and Au309 are shown.

core–shell cluster with a total of 309 atoms. This Cu147Ag162 cluster is then surrounded with empty spheres in the usual way as described in section 3. We have performed a SCF calculation in the ASA approximation of both the unrelaxed and relaxed structure obtained with the molecular dynamics procedure described in section 3. Figure 8 reports the ELNES spectra of the Cu L_3 edge of relaxed and unrelaxed Cu147Ag162. As reported in the previous section for Cu309, even in this case the effect of relaxation has only a small effect on the ELNES spectrum, mainly regarding a shift of about 0.3 eV of the first peak.

Figure 8 contains also the spectrum of Cu147 to allow a comparison with the ELNES of the core–shell cluster. There are clear variations in the behaviour of the spectrum due to the presence of the Ag shell. In order to disentangle the contributions from atoms in different shells, we have reported their spectra in figure 9. At lower energy loss (less than 10 eV from the onset) the spectra of inner atoms differ from that of Cu147 mainly for an energy shift of the whole spectrum, while the outer ones (in particular the spectrum of the outermost atoms) differ in shape. Note that in the case of the core–shell the variation of the 2p Cu core level energy among the different atoms of the clusters is in the range of 0.2 eV (to be compared to the 1.1 eV for Cu147).

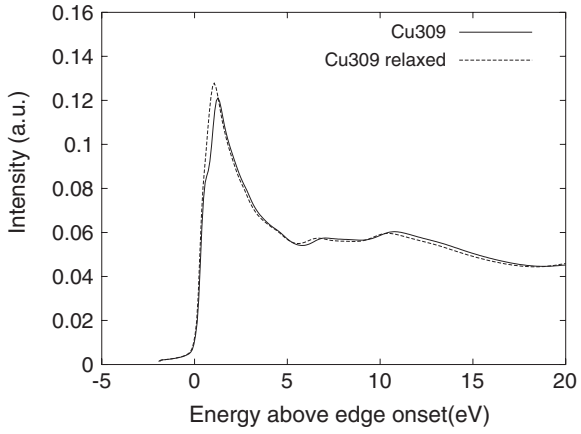

Figure 6. Comparison of the L_3 edge simulated for the relaxed and unrelaxed Cu309 cluster.

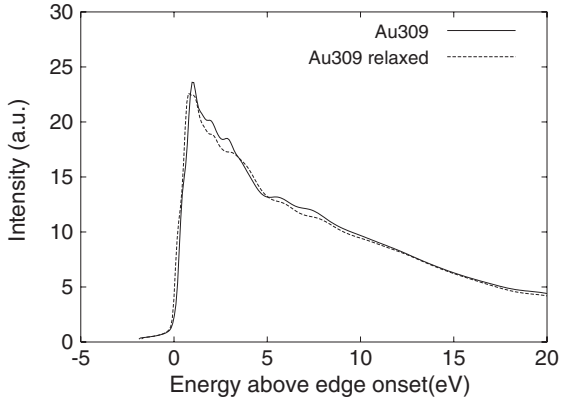

Figure 7. Comparison of the O_3 edge simulated for the relaxed and unrelaxed Au309 cluster.

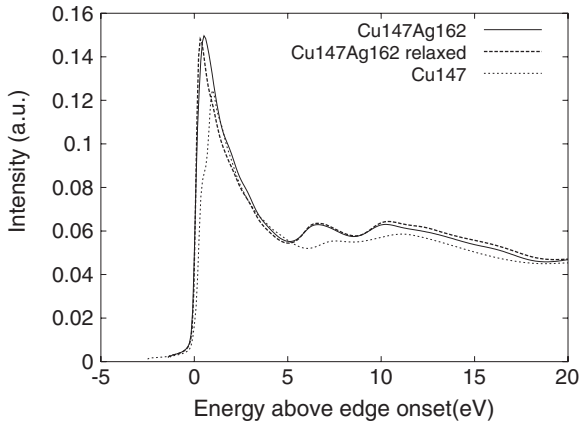

Figure 8. ELNES of the Cu L_3 edge simulated for the relaxed and unrelaxed Cu147Ag162 core–shell cluster. For comparison the spectrum of a Cu147 cluster is also shown.

5. Summary and conclusion

We have calculated ELNES spectra for copper and gold clusters with cuboctahedral symmetry using a multiple scattering approach. The use of symmetry allowed us to perform SCF calculations on quite big clusters (up to 923 atoms). So we have studied the influence of the size of the clusters on the shape of the ELNES spectra. We have also verified that the ASA

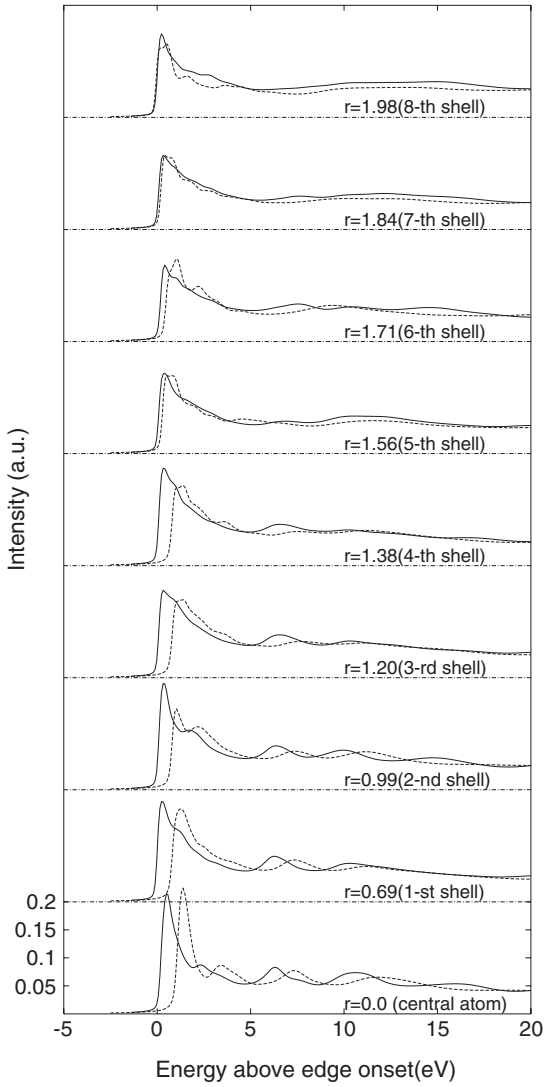

Figure 9. Contributions to the ELNES of the Cu L_3 edge of the relaxed core–shell cluster Cu147Ag162 (solid line) and cluster Cu147 (dashed line) from atoms with increasing distance from the centre. The radius r is given in units of the Cu bulk lattice parameter.

is a good approximation to simulate ELNES spectra for clusters with this symmetry (although a FP treatment is slightly more important when considering Au clusters). The introduction of structural relaxation of the clusters yields only small variations in the spectra (which even in this case are more pronounced for Au clusters). Nevertheless, the combination of both FP calculations and structure relaxation could have a significant influence on the shape of the spectra compared with an ASA simulation of an unrelaxed cluster. Therefore, when studying clusters made of materials different from the ones considered in this paper and/or with other point group symmetries, it would always be advisable to make a preliminary test on a cluster with a typical dimension of interest in order to check the importance of the structural relaxation and of the FP calculations.

Finally we have given an example of the ELNES of a Cu core–Ag shell cluster and we have shown the strong effect that the Ag shell determines on the ELNES with respect to the case of a 'bare' Cu cluster.

Clusters can be grown with various point group symmetries. For example Au clusters can have cuboctahedral, octahedral, truncated octahedral, icosahedral, decahedral structures, etc [34]. The formalism presented in this work can be straightforwardly applied to the above-mentioned structures so as to study the dependence of the ELNES on the cluster point group symmetry and dimension. Preliminary work of this kind has already been presented using non-SCF potentials [35]. In this way ELNES becomes a powerful tool for distinguishing the structure of single clusters. The extension of this work to core–shell clusters in order to study the nature of the interface between the core and the shell seems to be particularly interesting.

Acknowledgment

P H Dederichs is gratefully acknowledged for providing the original screened KKR code.

Appendix

We follow similar definitions reported in [36, 37]. The Green's function is

$$G(\boldsymbol{R}_i+\boldsymbol{r},\boldsymbol{R}_j+\boldsymbol{r}',E)=\sum_{LL'}R^i_L(\boldsymbol{r},E)G^{ij}_{LL'}(E)R^j_L(\boldsymbol{r}',E)+\delta_{ij}\sum_L R^i_L(\boldsymbol{r}_<,E)H^j_L(\boldsymbol{r}_>,E), \tag{A.1}$$

where $R^i_L(\boldsymbol{r},E)$ is the solution of the single-potential-scattering problem for a spherical wave $j_l(\kappa r)Y_L(\hat{\boldsymbol{r}})$ of angular momentum L incident on the general potential $V^i(\boldsymbol{r})$ of cell i. The wavefunctions $R^i_L(\boldsymbol{r},E)$ and the potentials $V^i(\boldsymbol{r})$ are expanded into real spherical harmonics:

$$R^i_L(\boldsymbol{r},E)=\sum_{L'}R^i_{L'L}(r,E)Y_{L'}(\hat{\boldsymbol{r}})\qquad V^i(\boldsymbol{r})=\sum_{L'}V_L(r)Y_{L'}(\hat{\boldsymbol{r}}). \tag{A.2}$$

Details on how to calculate the functions $R^i_{LL'}$ can be found in [36]. The presence of the nonspherical components $V_L(r)$ for $L\neq 0$ led to a coupled set of radial equations for the different partial waves $R^i_{LL'}$ which are solved with an iterative procedure. The behaviour of the total wavefunction $R^i_L(\boldsymbol{r},E)$ is dominated by the diagonal component $R_{LL}(r,E)$ which is roughly equals to the solution of a Schrödinger-like equation with the radial symmetric potential $V_{L=0}(r)$ (i.e. similar to the solution obtained in the ASA approximation).

Following as in section 2 we arrive at the same expression for $S(\boldsymbol{q},\boldsymbol{q},\Delta E)$ shown in equation (12) with $\mathbf{G}(E)$ given by equation (7) but with the following new definitions of the matrix elements:

$$\begin{aligned}M^{iA}_{LL'}(\boldsymbol{q})&=\int \mathrm{d}\boldsymbol{r}\,R^{ic}_L(r,E^i_c)Y_L(\hat{\boldsymbol{r}})(\boldsymbol{qr})R^i_{L'}(\boldsymbol{r},E)\\&=\sum_{L''}\int \mathrm{d}\boldsymbol{r}\,R^{ic}_L(r,E^i_c)Y_L(\hat{\boldsymbol{r}})(\boldsymbol{qr})R^i_{L''L'}(r,E)Y_{L''}(\hat{\boldsymbol{r}}),\end{aligned}$$

$$\begin{aligned}M^{iB}_{LL'}(\boldsymbol{q})&=2\int\int R^{ic}_L(r,E^i_c)Y_L(\hat{\boldsymbol{r}})(\boldsymbol{qr})R^i_{L'}(\boldsymbol{r},E)\\&\quad\times R^{ic}_L(r',E^i_c)Y_L(\hat{\boldsymbol{r}}')(\boldsymbol{qr}')H^i_{L'}(\boldsymbol{r}',E)\\&\quad\times\theta(r-r')\,\mathrm{d}\boldsymbol{r}\,\mathrm{d}\boldsymbol{r}'\\&=2\sum_{L1L2}\int\int R^{ic}_L(r,E^i_c)Y_L(\hat{\boldsymbol{r}})(\boldsymbol{qr})R^i_{L1L'}(r,E)Y_{L1}(\hat{\boldsymbol{r}})\end{aligned}$$

$$\times R_L^{ic}(r', E_c^i) Y_L(\hat{\boldsymbol{r}}')(\boldsymbol{q}\boldsymbol{r}') H^i_{L2L'}(r', E) Y_{L2}(\hat{\boldsymbol{r}}')$$
$$\times \theta(r - r')\, \mathrm{d}\boldsymbol{r}\, \mathrm{d}\boldsymbol{r}'. \tag{A.3}$$

In order to compare these results with the ones obtained in the ASA approximation, let us consider, for example, the matrix elements $M^{iA}_{LL'}(\boldsymbol{q})$. Now we have a sum of contributions from various $R_{L''L'}$, the most important being the diagonal one $R_{L'L'}$. All the other contributions due to the non diagonal angular momentum components of $R^i_{LL'}$ are a consequence of the non sphericity of the potentials. Since these functions are small in the region were the core function extends, their contributions to the matrix element is often negligible.

Finally, it is easy to find analogous expressions for the matrix elements given by equation (16).

References

[1] Wang Z L 2000 *J. Phys. Chem.* B **104** 1153
[2] Kadavanich A V, Kippeny T C, Erwin M M, Pennycook S J and Rosenthal S J 2001 *J. Phys. Chem.* B **105** 361
[3] Onida G, Reining L and Rubio A 2002 *Rev. Mod. Phys.* **74** 601
[4] Köstlmeier S 2001 *Ultramicroscopy* **86** 319
[5] Chelikowsky J R 2000 *J. Phys. D: Appl. Phys.* **33** R33
[6] Andersen O K 1975 *Phys. Rev.* B **12** 3060
Andersen O K and Jepsen O 1977 *Physica (Utrecht)* B **91** 317
[7] Inokuti M 1971 *Rev. Mod. Phys.* **43** 297
[8] Schattschneider P, Nelhiebel M and Jouffrey B 1999 *Phys. Rev.* B **59** 10959
[9] Kohl H and Rose H 1985 *Adv. Electron. Electron Phys.* **65** 173
[10] Zeller R 1997 *Phys. Rev.* B **55** 9400
[11] Braspenning P J and Lodder A 1994 *Phys. Rev.* B **49** 10222
[12] Kohn W and Sham L J 1965 *Phys. Rev.* **140** 1133A
[13] Lodder A and Braspenning P J 1994 *Phys. Rev.* B **49** 10215
[14] Zeller R, Dederichs P H, Újfalussy B, Szunyogh L and Weinberger P 1995 *Phys. Rev.* B **52** 8807
[15] Nelhiebel M, Luchier N, Schorsch P, Schattschneider P and Jouffrey B 1999 *Phil. Mag.* B **79** 941
[16] Durham P J, Pendry J B and Hodges C H 1982 *Comput. Phys. Commun.* **25** 193
[17] Natoli C R, Benfatto M and Doniach S 1986 *Phys. Rev.* A **34** 4682
[18] Durham P J 1981 *J. Phys. F: Met. Phys.* **11** 2475
[19] Ebert H 1996 *Rep. Prog. Phys.* **59** 1665
[20] Paxton A T, van Schilfgaarde M, Mac Kenzie M and Craven A J 2000 *J. Phys.: Condens. Matter* **12** 729
[21] Vosko S H, Wilk L and Nusair M 1980 *Can. J. Phys.* **58** 1200
[22] Koelling D D and Harmon B N 1977 *J. Phys. C: Solid State Phys.* **10** 3107
[23] Wildberger K, Lang P, Zeller R and Dederichs P H 1995 *Phys. Rev.* B **52** 11502
[24] Cleri F and Rosato V 1993 *Phys. Rev.* B **48** 22
[25] Haydock R 1980 *Solid State Phys.* **35** 215
[26] García de Abajo F J, Van Hove M A and Fadley C S 2001 *Phys. Rev.* B **63** 075404
[27] Wang Y, Stocks G M, Shelton W A, Nicholson D M C, Szotek Z and Temmerman W M 1995 *Phys. Rev. Lett.* **75** 2867
[28] Abrikosov I A, Niklasson A M, Simak S I, Johansson B, Ruban A V and Skriver H L 1996 *Phys. Rev. Lett.* **76** 4203
Abrikosov I A, Simak S I, Johansson B, Ruban A V and Skriver H L 1997 *Phys. Rev.* B **56** 9319
[29] Rijsenbrij D B B and Lodder A 1976 *J. Phys. F: Met. Phys.* **6** 1053
[30] Ries G and Winter H 1979 *J. Phys. F: Met. Phys.* **9** 1589
[31] Luitz J, Maier M, Hébert C, Schattschneider P, Blaha P, Schwarz K and Jouffrey B 2001 *Eur. Phys. J.* B **21** 363
[32] Hébert C, Kostner K and Schattschneider P 2000 *Proc. EUREM-Xii (Brno)* vol 3, p 333 (Edited by CS for Electron Microscopy)
[33] Andersen O K, Pawlowska Z and Jepsen O 1986 *Phys. Rev.* B **34** 5253
[34] Cleveland C L, Landman U, Schaaff T G, Shafigullin M N, Stephens P W and Whetten R L 1997 *Phys. Rev. Lett.* **79** 1873
[35] D'Agostino G and Gusso M 2003 *MRS Proc.* vol 788, ed S Komarneni, J C Parker and J J Watkins p 360
[36] Asato M, Settels A, Hoshino T, Asada T, Blügel S, Zeller R and Dederichs P H 1999 *Phys. Rev.* B **60** 5202
[37] Drittler B, Weinert M, Zeller R and Dederichs P H 1991 *Solid State Commun.* **79** 31